Catalysis Today 342 (2020) 79–87

Contents lists available at ScienceDirect

Catalysis Today

journal homepage: www.elsevier.com/locate/cattod

On the passivation of platinum promoted cobalt-based Fischer-Tropsch catalyst

Laura Fratalocchi, Gianpiero Groppi, Carlo Giorgio Visconti, Luca Lietti*, Enrico Tronconi*

Politecnico di Milano, Dipartimento di Energia, Via La Masa, 34, 20156, Milano, Italy

ARTICLE INFO

Keywords:
Cobalt catalyst
Fischer-Tropsch synthesis
Catalyst passivation
Cobalt reduction

ABSTRACT

Passivation of reduced cobalt-based catalysts is required prior to air exposure due to the exothermicity of the Co metal oxidation, which may lead to a significant increase of the temperature of the catalyst resulting in its degradation and in a potential fire hazard. This work shows the results of the passivation process carried out on a Pt-promoted Co-based catalyst supported on stabilized alumina at different space velocities in the range of 5–50 Ncc/min/g_{cat} and constant O_2 concentration of 1 vol.%. Increasing the O_2 flow fed to the reactor, the specific amount of O_2 consumed on the catalyst slightly decreases. Around 30% of Co metal particles are oxidized to CoO species in all the passivation treatments. These species are found to be much more reducible than the Co oxides species present on the calcined catalyst. Indeed, all the passivated catalysts are completely depassivated at a temperature which is significantly lower (300 °C) than that needed to fully reduce the calcined catalyst (400 °C). The temperature of the catalyst almost linearly increases with the increase of the O_2 feed flow. Indeed, an abrupt increase of the catalyst temperature is observed for high O_2 flows, resulting in a decrease of the Co° dispersion (i.e. increase of the average Co° crystallites size) after depassivation. This result is explained with the onset of sintering phenomena of the CoO species formed during passivation. The passivation treatment is found to be unsuitable for long-term catalyst protection, since a deep re-oxidation of the passivated catalyst is observed after two months of air exposure. The effectiveness of the catalyst passivation is eventually validated by running FT reactivity tests at industrially relevant process conditions. The activity of the calcined catalyst reduced in-situ at 400 °C is compared to that of the same catalyst reduced ex-situ at the same temperature, passivated at low O_2 flow and depassivated in-situ at 300 °C. Interestingly, similar stability and reactivity, expressed both in terms of activity and selectivity, are obtained.

1. Introduction

Supported cobalt is the catalyst of choice for the low temperature Fischer-Tropsch synthesis (LT-FTS) step in the gas to liquid processes (GTL), due to its high activity and selectivity to long-chain hydrocarbons [1]. In such systems, it is generally accepted that the active sites are metallic Co sites [2], thus the activation of the catalyst prior to reaction is required. Activation involves the reduction of the catalyst under H_2-flow at pressure of 0.8–1.3 bar and temperature of 400–450 °C [3].

The reduction of the catalyst in the synthesis reactor (*in-situ* reduction) has several constrains, such as the loss of several days of production and the availability of specially designed reactor units able to reach the process conditions requested for the catalyst activation. In this regard, several industrial patents [3–7] report the *ex-situ* reduction of the catalyst, i.e. carried out in a different reactor with respect to that adopted for the FTS, followed by a passivation step. The advantage is that the passivated catalyst is transferred into the FTS unit and depassivated *in-situ* prior to the reaction under milder conditions. For instance, in a patent by Sasol [3] the ex-situ reduction of the calcined catalyst is carried out at 425 °C while the in-situ depassivation at 250–300 °C.

The passivation of the reduced catalyst is crucial due to the high oxidability of the cobalt metal species upon exposure to air and the high exothermicity of this reaction [8]. Indeed, the reduced catalyst exposed to air may be damaged by sintering and may constitute a fire hazard during the transfer in the FTS unit [3].

The passivation treatment involves the formation of a thin oxide layer protecting the metallic core from further oxidation in air and allows the storage of the sample under ambient conditions [8,9]. The passivation process is commonly carried out at ambient temperature by feeding a low concentration of O_2, typically in the range 0.1–1% [9].

* Corresponding authors.
E-mail addresses: luca.lietti@polimi.it (L. Lietti), enrico.tronconi@polimi.it (E. Tronconi).

https://doi.org/10.1016/j.cattod.2019.02.069
Received 5 November 2018; Received in revised form 28 January 2019; Accepted 24 February 2019
Available online 25 February 2019

Besides O_2, a mildly oxidising gaseous atmosphere of CO_2 was recently proposed for the passivation of a Co-based FT catalyst [9] although the results were not satisfactory [9]. CO and CO/H_2 mixtures were also proposed as passivating agents [8] through the formation of a carbidic carbon layer and of carbonaceous species on the surface of the catalyst, respectively. However, the subsequent depassivation step did not lead to the recovery of the original activity of the calcined catalyst due to the conversion of carbidic carbon to graphitic carbon [8].

In the scientific literature, passivation treatments are widely applied to preserve reduced or spent FT catalysts during their transfer from the reactor to characterization instruments [9–17], but only few studies deal with the effectiveness of these passivation treatments [9]. Furthermore, none of these works compares the catalytic performances in the FTS of the calcined catalyst reduced in-situ and the calcined catalyst reduced and passivated ex-situ and then depassivated in-situ.

In this work, the O_2-passivation/depassivation of a Pt-promoted Co-based catalyst supported on stabilized alumina is investigated both through the different characterization techniques and the assessment of its FTS catalytic performances at industrially relevant operating conditions. In particular, the reactivity of a *ex-situ* passivated and *in-situ* depassivated catalyst is compared with that of an *in-situ* reduced sample.

2. Material and methods

2.1. Catalyst preparation

A Pt-promoted cobalt-based catalyst ($Co/Pt/Al_2O_3{}^{(s)}$) was used in this study. It was prepared following the procedure reported in [18]. Briefly, the first step of the catalyst synthesis protocol is the stabilization of the γ-Al_2O_3 support with a protective layer of cobalt aluminate species [19,20]. To this end, γ-Al_2O_3 spheres (Sasol Puralox®, d_{pellet} = 300 μm) were impregnated (incipient wetness impregnation, IWI, method) with an aqueous solution of $Co(NO_3)_2{\cdot}6H_2O$ (Sigma Aldrich, 98 wt.%) so to reach a Co loading of ≈5.7 wt.%. Then, the impregnated support was dried at 120 °C for 1 h and calcined in static air at 900 °C for 4 h (heating rate: 1.5 °C/min) to form $CoAl_2O_4$ species at the γ-Al_2O_3 surface [19,20]. The stabilized support will be referred in the following as $Al_2O_3{}^{(s)}$. As shown in our recent works [19,20], $Al_2O_3{}^{(s)}$ is inactive in the FTS.

Then ≈0.1 wt.% of Pt was impregnated on the $Al_2O_3{}^{(s)}$ support by incipient wetness impregnation using an aqueous solution of 3.4 wt.% $Pt(NH_3)_2{\cdot}(NO_2)_2$ in NH_4OH (Sigma Aldrich, 99 wt.%). The impregnation step was followed by drying in static air at 120 °C for 2 h (heating rate: 2 °C/min) and calcination at 500 °C for 4 h (heating rate: 2 °C/min).

The obtained $Pt/Al_2O_3{}^{(s)}$ sample was impregnated four times with an aqueous solution of $Co(NO_3)_2{\cdot}6H_2O$ so to reach an active Co loading of ≈19 wt.%. After each impregnation step, the sample was first dried in static air at 120 °C for 2 h (heating rate: 2 °C/min) and then calcined in static air at 500 °C for 4 h (heating rate: 2 °C/min) [18]. $Co/Pt/Al_2O_3{}^{(s)}$ catalyst was calcined at 500 °C in total 16 h.

2.2. Catalyst passivation

Passivation experiments were carried out in a lab-scale rig equipped with a quartz reactor (1 cm I.D. and 40 cm long) placed into a tubular electric furnace. Mass flow controllers (Brooks Instrument, 5850) were used to regulate the flow rates of the reactants. The gases exiting the reactor were analyzed by using an on-line gas micro-gaschromatograph (Pollution GCX) equipped with a molsieve 5 Å column connected to a thermal conductivity detector (TCD). This enables to monitor the amount of O_2 consumed during passivation. Blank tests were also carried out prior to each passivation experiment by replacing the catalyst bed with inert α-Al_2O_3 powder.

In a typical experiment, ≈1 g of catalyst was loaded into the reactor and a K-type thermocouple was positioned at the centre of the catalytic bed. The catalyst was reduced at 400 °C for 17 h with a heating rate of 2 °C/min from room temperature to 400 °C and at atmospheric pressure under a flow of 83.33 $Ncc/min/g_{cat}$ of pure H_2. These operating conditions will be referred to in the following as "standard reduction conditions" [18–20]. Afterwards, the catalyst was cooled down to room temperature in N_2 (83.33 $Ncc/min/g_{cat}$). The reduced catalyst was then passivated by feeding 1 vol.% O_2 in He at different space velocities of 5, 11, 20, 30, 40 and 50 $Ncc/min/g_{cat}$. During this step, the temperature of the catalyst bed was monitored in order to verify as to whether exotherms occurred during the exposure to oxygen.

Each experiment was repeated at least four times, in order to evaluate the reproducibility of the results in terms of O_2 consumption and variation of the catalyst temperature. Accordingly, standard deviations were calculated both for the total amount of O_2 consumed by the catalyst in each experiment and on the variation of the catalyst temperature during passivation. Standard deviations around 1.2% were obtained for the total amount of O_2 consumed at space velocity of 20 $Ncc/min/g_{cat}$ and above, while slightly higher values (close to 3%) were obtained at lower space velocities. Standard deviations lower than 1% were calculated for the variation of the catalyst temperature during passivation for all replicated experiments.

2.3. Catalyst characterization

The BET area (S_{BET}) and the specific pore volume (V_p) of the starting γ-Al_2O_3 material, the $Al_2O_3{}^{(s)}$ and $Pt/Al_2O_3{}^{(s)}$ supports and the calcined $Co/Pt/Al_2O_3{}^{(s)}$ catalyst (i.e. after calcination) were estimated from the N_2 adsorption isotherms measured at −196 °C in a Micromeritics Tristar 3000 instrument. Prior to the measurements, samples were heated at 120 °C for 3 h at 0.1 Torr. The average pore size (d_p) and the pore size distribution were calculated from the adsorption branch of the isotherm using the BJH method.

The actual Pt and Co loadings on the calcined catalysts were determined by inductively coupled plasma mass spectrometry (Thermo Electron, X series 2 ICP-MS) on the samples dissolved in ultrapure concentrated nitric acid (Sigma Aldrich, 70%). The actual Co loading of the catalyst obtained by ICP-MS analyses is inclusive of the amount of cobalt used for the support stabilization.

XRD measurements were carried out by using a Bruker D8 Advanced diffractometer, with a CuK_α radiation and a scintillation detector. The powder diffractograms of the samples were collected over a 2θ range of 25–70° at a step time of 12.5 s. XRD analyses allowed the identification of the cobalt phases present on the samples. The Co_3O_4 average crystallite size of the calcined catalyst was estimated by using the Scherrer equation from the diffraction peak at 2θ = 37.06° [21], obtained after subtraction of the $Al_2O_3{}^{(s)}$ diffraction pattern from that of the $Co/Pt/Al_2O_3{}^{(s)}$ catalyst.

H_2-temperature programmed reduction (H_2-TPR) analyses were carried out on various samples (calcined, passivated, reduced, depassivated) using a Micromeritics Thermoquest TPDRO1100 instrument. The instrument is equipped with a thermal conductivity detector (TCD) located downstream the reactor after a soda lime steam trap. In a typical experiment, the sample was heated from 40 to 1050 °C (heating rate: 15 °C/min) under a flow of 5.15 vol.% H_2 in Ar (600 $Ncc/min/g_{cat}$).

The reduction and the depassivation of the calcined and passivated catalysts, respectively, used for TPR analysis was carried out in the TPDRO1100 instrument under a flow of pure H_2 (83 $Ncc/min/g_{cat}$) and atmospheric pressure. The samples were reduced at 400 °C for 17 h or at 300 °C for 17.83 h (heating rate: 2 °C/min), so to maintain the same length of the reducing treatment. After reduction, the sample was cooled to 40 °C in Ar and the reactor was purged with a stream of 5.15 vol.% H_2 in Ar and further heated to 1050 °C (heating rate: 15 °C/min). H_2 consumption in this TPR analysis corresponds to the amount of cobalt which remains unreduced after the treatment in H_2 at 300 or

400 °C.

Information on the Co° dispersion of the catalysts were collected running H_2-chemisorption experiments using the same TPDRO instrument which was used to run TPR experiments. To this end, 300 mg of sample were placed in a quartz reactor and reduced in situ at 300 or 400 °C After flowing Ar at the set reduction temperature for 2 h and cooling to 100 °C, successive pulses of H_2 (264 μL/pulse) were sent to the catalyst.

The total amount of chemisorbed hydrogen (mol_{H2}^{chemi}) was calculated from the difference between the peak area obtained during the saturation experiment and the areas of the peaks in the absence of a chemisorption event. Then, by assuming a chemisorption stoichiometry of Co:H equal to 1, the cobalt metal dispersion (D, [%]) was calculated as per Eq. (1)

$$D\ [\%] = \frac{(mol_{H2}^{chemi}/g_{cat}) \cdot 2}{mol_{Co^0}^{TPR}/g_{cat}} .100 \quad (1)$$

where mol_{H2}^{chemi}/g_{cat} is the total amount of H_2 chemisorbed in the experiment and $mol_{Co^0}^{TPR}/g_{cat}$ is the amount of metallic cobalt on the reduced catalysts.

The average cobalt metal crystallite size (dCo_{chemi}^0) was estimated from the Co° dispersion measurements using Eq. (2) [22]:

$$dCo_{chemi}^0\ [nm] = \frac{96}{D\ [\%]} \quad (2)$$

2.4. Catalytic tests

The catalysts were tested in the FTS using a fixed bed tubular reactor (1.1 cm ID) after dilution with α-Al_2O_3 pellets of the same granulometry, so as to prevent local hot-spots (catalyst: alumina = 1:4 v/v). More details on the reactor and on the used lab-scale apparatus can be found in [23] and references therein. Catalytic runs were carried out at relevant process conditions: T = 200 °C, P = 25 bar, H_2/CO inlet molar ratio = 2.0, GHSV = 106.8 Ncc/min/g_{cat}, inerts (N_2+ Ar) in the feed = 24 vol.%.

The performances of two samples were compared: (i) the Co/Pt/$Al_2O_3^{(s)}$ catalyst reduced in-situ in the FTS unit at the standard reduction conditions and (ii) the Co/Pt/$Al_2O_3^{(s)}$ catalyst reduced at the same process conditions, passivated with 11 Ncc/min/g_{cat} of 1 vol.%O_2/He, transferred in the FTS unit and depassivated in-situ using 83.33 Ncc/min/g_{cat} of pure H_2 at 300 °C for 17.83 h with an heating ramp from room temperature to 300 °C of 2 °C/min.

The unconverted reactants and the full spectrum of products were measured by on-line and off-line gas-chromatography. Details on the product sampling and analysis procedures can be found elsewhere [24]. In order to collect representative activity data, both the catalysts studied in this work were tested for more than 90 h. In order to check the achievement of steady state conditions, multiple data at the same experimental condition were collected for more than 48 consecutive hours. Data were considered steady when the CO conversion (X_{CO} [%], Eq. (3)) and the selectivity to the main FTS products (S_i [%], Eq. (4)) varied within less than 5% in 48 h.

$$X_{CO}\ [\%] = \left(1 - \frac{F_{CO}^{out}}{F_{CO}^{in}}\right).100 \quad (3)$$

$$S_i\ [\%] = \left(\frac{F_i^{out} \cdot n_i}{\sum_i^{NP} (F_i^{out} \cdot n_i) + F_{CO2}^{out}}\right).100 \quad (4)$$

F_i^{out} is the molar productivity of ith hydrocarbon species, n_i is the carbon atom number of the ith species and NP is the number of the hydrocarbon products (paraffins C_1–C_{49} and olefins C_2–C_{17}) identified at the reactor outlet. The selectivity to carbon dioxide was calculated as in Eq. (5):

Table 1
Textural properties of the samples.

	S_{BET}[a] [m^2/g]	V_p[a] [cm^3/g]	d_p[b] [nm]	Co loading[c] wt.%	Pt loading[c] wt.%
γ-Al_2O_3	145	0.43	12	–	–
$Al_2O_3^{(s)}$	102	0.37	14	5.57 ± 0.11	–
Pt/$Al_2O_3^{(s)}$	102	0.37	14	5.60 ± 0.10	0.141 ± 0.004
Co/Pt/$Al_2O_3^{(s)}$	59	0.20	14	22.80 ± 0.59	0.110 ± 0.002

[a] BET measurements.
[b] BJH analysis.
[c] ICP-MS analysis.

$$S_{CO2}\ [\%] = \left(\frac{F_{CO2}^{out}}{F_{CO}^{in} - F_{CO}^{out}}\right).100 \quad (5)$$

Carbon balances, calculated as moles of C contained in the reaction products divided by the moles of CO converted (Eq. (6)), always closed within ± 5%.

$$C.\ B.\ (1) = \frac{\sum_{i \neq CO} F_{i,products}^{out} \cdot n_i}{F_{CO}^{in} - F_{CO}^{out}} (n_i = 1 - 49) \quad (6)$$

3. Results and discussion

3.1. Characterization of the calcined materials

The textural properties of the calcined Co/Pt/$Al_2O_3^{(s)}$ catalyst and of the starting precursors (γ-Al_2O_3 pellets, stabilized alumina $Al_2O_3^{(s)}$ and Pt/$Al_2O_3^{(s)}$) are shown in Table 1. Both BET area and pore volume of the $Al_2O_3^{(s)}$ support are about 30% lower than those of the starting γ-Al_2O_3 pellets. The decrease of the BET area is due to the high-temperature stabilization procedure (900 °C), while the decrease of the pore volume to the Co impregnation. $Al_2O_3^{(s)}$ and Pt/$Al_2O_3^{(s)}$ show similar textural properties, thus indicating no effect of the Pt-impregnation step and following thermal treatments. The BET area obtained with the Co/Pt/$Al_2O_3^{(s)}$ catalyst is almost half compared to those of the support. The decrease of the surface area is accompanied by a decrease of the pore volume as well, whereas the pore diameter is rather constant. The pore size distributions (not shown) exhibit a narrow pore size distribution in the mesopore range (Table 1).

The values on the effective composition of the samples obtained by ICP-MS analysis are in good agreement with the nominal Co and Pt loadings of the support and the catalyst.

Fig. 1 shows the diffraction patterns of the $Al_2O_3^{(s)}$support and the calcined Co/Pt/$Al_2O_3^{(s)}$catalyst. The calcination at 900 °C used for the preparation of the $Al_2O_3^{(s)}$ pellets causes the interaction of cobalt-containing species with the alumina support, resulting in the formation of cobalt aluminates (main peaks at 31.5 and 37°), whose diffraction peaks overlap with those of Co_3O_4. The diffraction pattern of the Co/Pt/$Al_2O_3^{(s)}$catalyst shows peaks associated with the presence of the Co_3O_4 phase (Fig. 1). The average size of Co_3O_4 crystallites, estimated by applying the Scherrer equation to the most intense Co_3O_4 diffraction peak at 2θ = 37.06° [21] after the subtraction of the pattern of the support is 18 nm, from which a Co° crystallite size of 13.5 nm can be determined [25].

The results of H_2-TPR measurements performed on the calcined catalyst are shown in Fig. 2(a). Three distinct reduction peaks can be identified in the TPR profile of the catalyst, corresponding to the following reduction processes (Eqs. 7–9):

$$Co_3O_4 + H_2 \rightarrow 3CoO + H_2O \quad (7)$$

$$3CoO + 3H_2 \rightarrow 3CoO + 3H_2O \quad (8)$$

$$CoAl_2O_4 + H_2 \rightarrow Co^0 + Al_2O_3 + H_2O \quad (9)$$

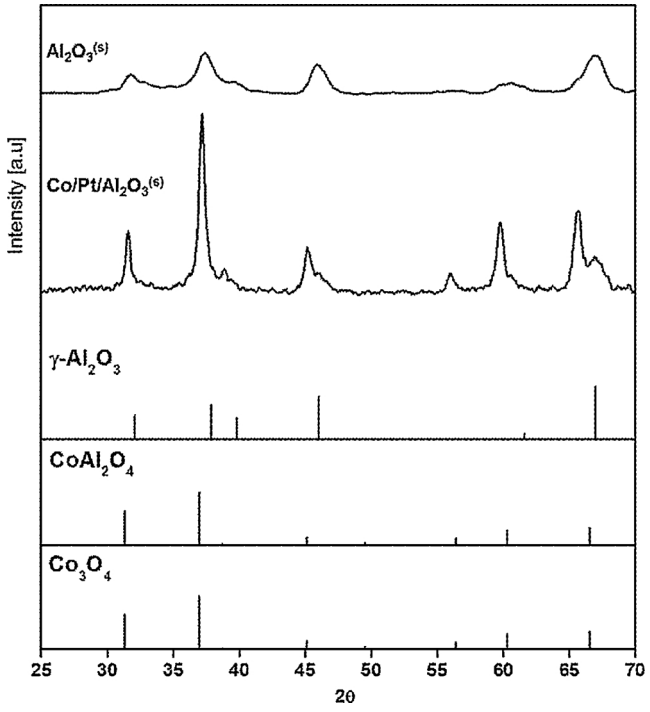

Fig. 1. XRD patterns of $Al_2O_3^{(s)}$ support and calcined $Co/Pt/Al_2O_3^{(s)}$ catalyst. The reference patterns of γ-Al_2O_3, Co_3O_4 and $CoAl_2O_4$ are also shown.

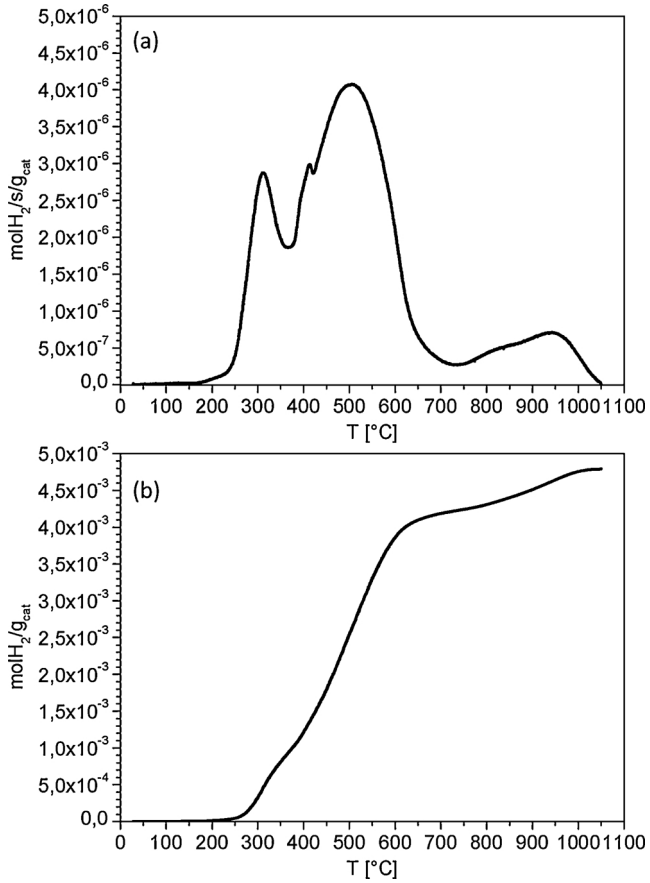

Fig. 2. H_2-TPR profiles of (a) the calcined $Co/Pt/Al_2O_3^{(s)}$ catalyst and (b) integral H_2 consumptions as a function of the temperature.

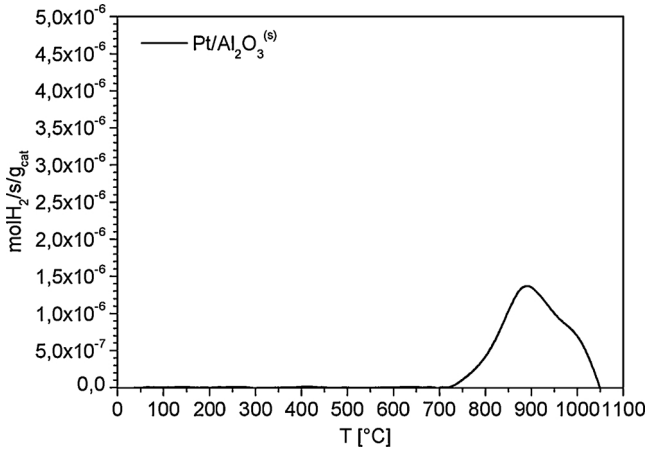

Fig. 3. H_2-TPR profiles of the calcined Pt-doped stabilized support ($Pt/Al_2O_3^{(s)}$).

The first peak with a maximum detected at 301 °C is associated with the reduction of the Co_3O_4 species to CoO (Fig. 2(a)) [18,20,26]. The following peak with a maximum at 511 °C is associated with the reduction of CoO to metallic Co (Fig. 2(a)) [18,20,26], while the small peak near 420 °C is very likely associated to same heterogeneity of the Co oxide phase. Fig. 2(b) shows the integral amount of H_2 consumed during the TPR run. Notably, a good agreement between the total amount of H_2 consumed in the TPR profile of the calcined $Co/Pt/Al_2O_3^{(s)}$ catalyst at 700 °C and the theoretical amount of H_2 needed to reduce Co_3O_4 species to Co° ($4.1{\cdot}10^{-3}$ vs. $4.3{\cdot}10^{-3}$).

Eventually, the last peak in the TPR profile with maxima at 827 and 923 °C involves the reduction of Co^{x+} species highly interacting with the support (Fig. 2(a)), i.e. the $CoAl_2O_4$ species present in the $Al_2O_3^{(s)}$ support. In fact, a good agreement is obtained also in this case between the amount of H_2 consumed under these peaks and the theoretical amount of H_2 needed to reduce the Co aluminates ($6.4{\cdot}10^{-4}$ vs. $6.9{\cdot}10^{-4}$). Besides, the H_2-TPR profile obtained with the $Pt/Al_2O_3^{(s)}$ support (Fig. 3) shows the onset of only one reduction peak at temperatures over 700 °C, in line with the reduction of $CoAl_2O_4$ species [19].

3.2. Characterization of the calcined $Co/Pt/Al_2O_3^{(s)}$ catalyst reduced at 300 °C and at 400 °C

The H_2-TPR profiles of the $Co/Pt/Al_2O_3^{(s)}$ catalyst reduced in-situ at 300 °C and at 400 °C are shown in Fig. 4. The H_2-TPR profiles of the calcined $Co/Pt/Al_2O_3^{(s)}$ catalyst is also shown for comparison purposes.

After reduction at 400 °C, the peaks assigned to the reduction from Co_3O_4 to CoO and from CoO to Co° completely disappear, thus pointing out the complete reduction of the catalyst. The peaks observed at high temperature match closely with those observed in the TPR profiles of the calcined catalyst (Fig. 4), thus indicating that the $CoAl_2O_4$ species used for the support stabilization are not reducible at the adopted reduction conditions [20].

In the case of the $Co/Pt/Al_2O_3^{(s)}$ sample reduced in-situ at 300 °C, the peak assigned to the $Co^{3+} \rightarrow Co^{2+}$ reduction completely disappears, suggesting that Co_3O_4 species are not present even if the reduction treatment is performed at lower temperature. At variance, the CoO to Co° reduction peak is still partially present, indicating an incomplete reduction of this sample. This is in line with the fact that the transition from Co^{2+} to Co° is known to be more difficult that from Co^{3+} to Co^{2+} [26].

The fraction of unreduced CoO particles is possibly related to the smallest particles present on the catalyst, which are known to be hardly reducible [20,26]. With the assumption that the unreduced cobalt is mainly in the Co^{2+} oxidation state, the degree of reduction of the

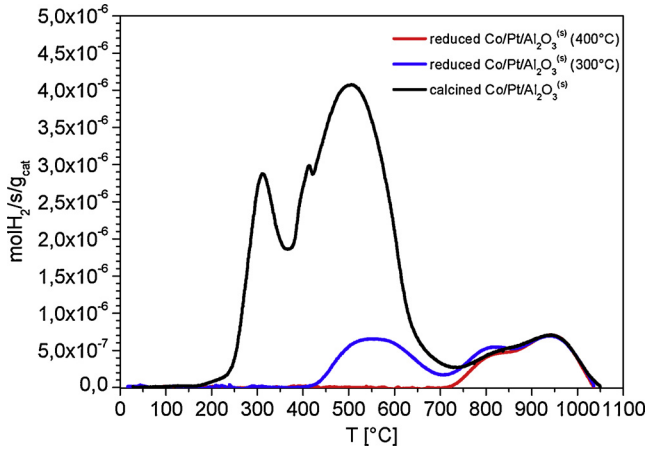

Fig. 4. H_2-TPR profiles of the $Co/Pt/Al_2O_3^{(s)}$ catalyst reduced at 400 °C (red line) and at 300 °C (blue line) as a function of the temperature. H_2-TPR profiles of the calcined $Co/Pt/Al_2O_3^{(s)}$ catalyst is also shown (black line). (For interpretation of the references to colour in this figure legend, the reader is referred to the web version of this article).

samples can be calculated as the ratio between the amount of H_2 consumed to fully reduce the residual CoO species and the amount of H_2 required to reduce all the starting Co_3O_4 species into Co°. The degree of reduction of the catalysts is found to be 100 and 77% after reduction at 400 and 300 °C, respectively. As already observed with the catalyst reduced at 400 °C, the reduction peaks of the Co-aluminates are still present.

The dispersion of the active Co metal centers (D, Eq. (1)) on the catalytic surface of the $Co/Pt/Al_2O_3^{(s)}$ catalyst after reduction at 400 °C, which is measured via H_2-chemisorption, is 11.6%, from which a value of 8.3 nm of Co° crystallites size can be calculated (dCo°, Eq. (2)) (Table 2). This value is lower than the expected value of 13.5 nm estimated from the contraction [25] of the Co_3O_4 particles having size of 18 nm (see above). This is likely related to the presence of Pt that enables the reduction of the very small Co_3O_4 crystallites present on the catalyst surface not detected in the XRD analysis of the calcined sample, also because of the partial overlapping of Co_3O_4 and $CoAl_2O_4$ reflections.

The Co° dispersion (D, Eq. (1)) calculated on the $Co/Pt/Al_2O_3^{(s)}$ catalyst reduced at 300 °C is 6.4%, from which a value of the Co° crystallites size near 15 nm can be calculated from Eq. (2) (Table 2). This value is in line with the expected value of 13.5 nm. From these data it clearly appears that the decrease of the reduction temperature affects the Co° dispersion (i.e. number of active Co° surfaces sites), which results halved with respect to the standard reduction temperature of 400 °C A minor effect on the catalyst reducibility is instead observed. This indicates that highly dispersed Co° crystallites are present on the surface after reduction at 400 °C; these species do not form if the catalyst is reduced at 300 °C.

Table 2
H_2-chemisorption results.

	D[a] [%]	d_{Co}[b] [nm]
$Co/Pt/Al_2O_3^{(s)}$(red@400 °C)	11.6	8.3
$Co/Pt/Al_2O_3^{(s)}$(red@300 °C)	6.4	15
$Co/Pt/Al_2O_3^{(s)}$ passivated at 5-11-20 Ncc/min/g_{cat} (red@400 °C)	12.0	8.0
$Co/Pt/Al_2O_3^{(s)}$ passivated at 5-11-20 Ncc/min/g_{cat} (red@300 °C)	12.5	7.7
$Co/Pt/Al_2O_3^{(s)}$ passivated at 30.5 Ncc/min/g_{cat} (red@400 °C)	10.0	9.6
$Co/Pt/Al_2O_3^{(s)}$ passivated at 40 Ncc/min/g_{cat} (red@400 °C)	8.4	11.4
$Co/Pt/Al_2O_3^{(s)}$ passivated at 50 Ncc/min/g_{cat} (red@400 °C)	7.8	12.3

[a] Co metal dispersion calculated in Eq.(1).
[b] Co metal crystallites size calculated in Eq.(2).

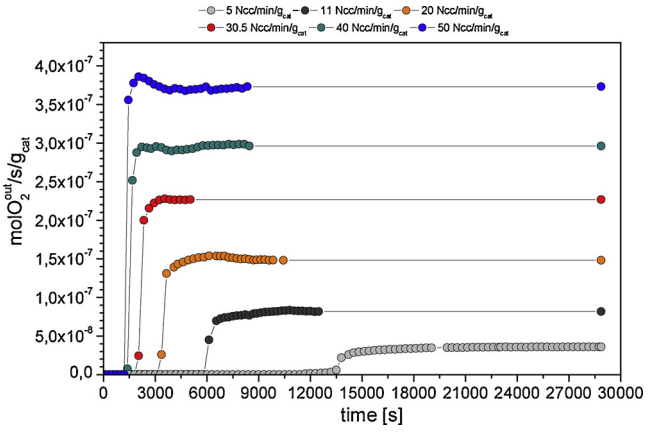

Fig. 5. Outlet molar flow of O_2 ($molO_2^{out}/s/g_{cat}$) monitored during the passivation treatment carried out at different $GHSV_{O2/He}$ as a function of the time (inlet of the O_2 flow at time 0 s). (For interpretation of the references to colour in this figure legend, the reader is referred to the web version of this article).

3.3. Catalyst passivation

The outlet O_2 molar flow ($molO_2^{out}/s/g_{cat}$) monitored during the passivation treatment of the catalyst at $GHSV_{O2/He}$ of 5, 11, 20, 30.5, 40 and 50 Ncc/min/g_{cat} is shown in Fig. 5.

The O_2 profiles show a typical adsorption behavior, the concentration being zero until a breakthrough time is observed where a sudden transition to an asymptotic level equal to the inlet concentration occurs. The breakthrough time proportionally decreases on increasing the GHSV (i.e. the specific O_2 molar flow rate), consistently with a constant adsorption capacity. Actually, the specific amount of O_2 consumed ($molO_2^{cons}/g_{cat}$) upon passivation slightly decreases with the space velocity (Fig. 6).

The temperature evolution with time measured at the center of the catalyst bed during the passivation is shown in Fig. 7. The temperature remains almost constant when the passivation step is performed at low $GHSV_{O2/He}$ of 5 and 11 Ncc/min/g_{cat}. In fact the temperature gradient (ΔT), defined as the difference between the maximum and the minimum temperature recorded during passivation, is around 1 and 2.5 °C at $GHSV_{O2/He}$ of 5 and 11 Ncc/min/g_{cat}, respectively. At variance, stronger ΔTs are obtained at higher O_2/He space velocity. Indeed ΔT values near 5.3, 8.5, 11.9 and 17.5 °C are obtained at GHSV = 20, 30.5, 40 and 50 Ncc/min/g_{cat}, respectively.

To better analyze the process, passivation experiments carried out at

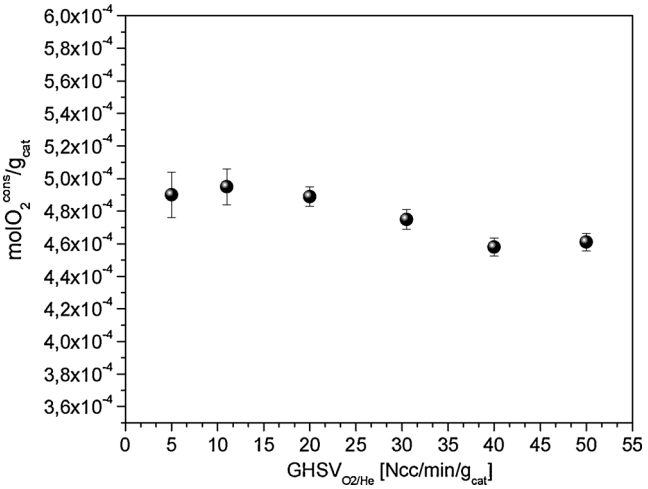

Fig. 6. O_2 consumed ($molO_2^{cons}/g_{cat}$) in the passivation treatment carried out at different $GHSV_{O2/He}$.

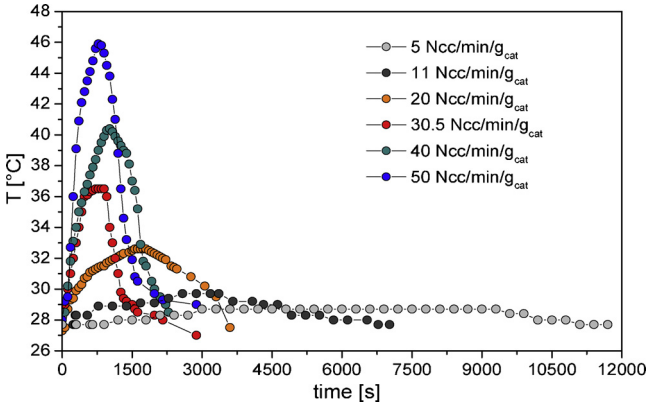

Fig. 7. Temperature of the catalyst bed measured during the passivation treatment carried out at different $GHSV_{O2/He}$ as a function of the time. (For interpretation of the references to colour in this figure legend, the reader is referred to the web version of this article).

the lowest space velocities (i.e. at $GHSV_{O2/He}$ of 5, 11 and 15 Ncc/min/g_{cat}) have been repeated by increasing the catalyst loading from 1 to 2 g. The total amount of O_2 consumed normalized to the gram of catalyst ($molO_2^{cons}/g_{cat}$) does not change, but an increase in the ΔTs could be observed at the same space velocity when increasing the catalyst loading (Fig. 8(a)). In fact the ΔTs increases from 1 to 3 °C by doubling the catalyst loading at GHSV = 5 Ncc/min/g_{cat} and from 2.5 to 6.5 °C at GHSV = 11 Ncc/min/g_{cat}. This can be explained by considering that during the initial part of the experiments, O_2 is completely consumed. Accordingly the heat released (and hence the ΔT) depends almost linearly on the oxygen feed only, and not on the catalyst loading. As a matter of facts, as shown in Fig.8(b), the observed ΔTs depends on the O_2-flow and not on the catalyst weight.

This result is relevant in view of the scale up of the passivation process to the industrial scale, where reactor of larger size loaded with higher amounts of catalyst and operated at higher O_2 flow rates may results in stronger thermal effects. This implies that the passivation process must be carried out at controlled operating conditions (low O_2 flow) and in highly thermally efficient systems able to easily remove the heat of reaction.

3.4. Characterization of the passivated catalysts

The sample passivated with $GHSV_{O2/He}$ of 11 Ncc/min/g_{cat} was investigated by XRD, and the results are shown in Fig. 9. Reflections attributable to Co° species are distinguishable (main diffraction peak at 2θ = 44.6°), whereas peaks associated to other species (e.g. CoO main reflection at 2θ ~ 42.8°) are hardly detectable. This possibly indicates a layer thickness close to the lower detection limit for crystallites sizes being around 2 nm and/or to the presence of a partially amorphous

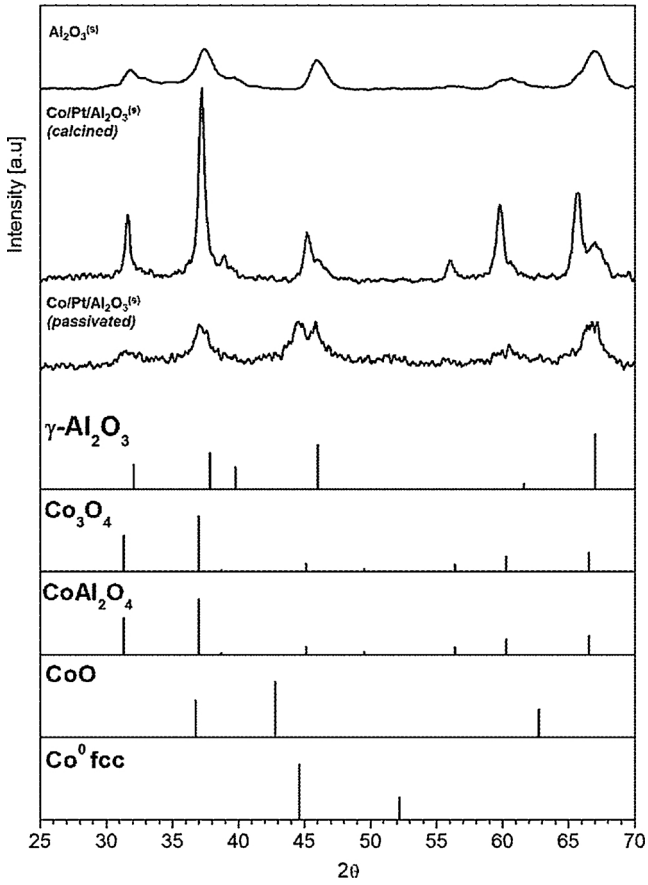

Fig. 9. XRD patterns of the $Al_2O_3^{(s)}$ support, the calcined $Co/Pt/Al_2O_3^{(s)}$ catalyst and the catalyst after passivation with a $GHSV_{O2/He}$ of 11Ncc/min/g_{cat} ($Co/Pt/Al_2O_3^{(s)}$(P)).
The reference patterns of γ-Al_2O_3, Co_3O_4, $CoAl_2O_4$, CoO and Co° are also shown.

Co_xO_y shell as reported in literature [9]. Due to the poor signal/noise ratio in the diffraction patterns of the passivated catalyst, a quantitative estimation about the CoO and Co° crystallites size cannot be given.

It is reasonable that the $CoAl_2O_4$ peaks detected on this sample are those belonging to the stabilized support, as in the case of the calcined $Co/Pt/Al_2O_3^{(s)}$ catalyst. However, since these peaks partially overlap with those related to the Co_3O_4 phase, the presence of these species cannot be excluded.

H_2-TPR analyses were performed on all the passivated catalysts, and results are shown in Fig. 10. The analyses were carried out immediately after (≈ 10 min) the sample was unloaded from the reactor. No increase of the catalyst temperature was recorded in the subsequent

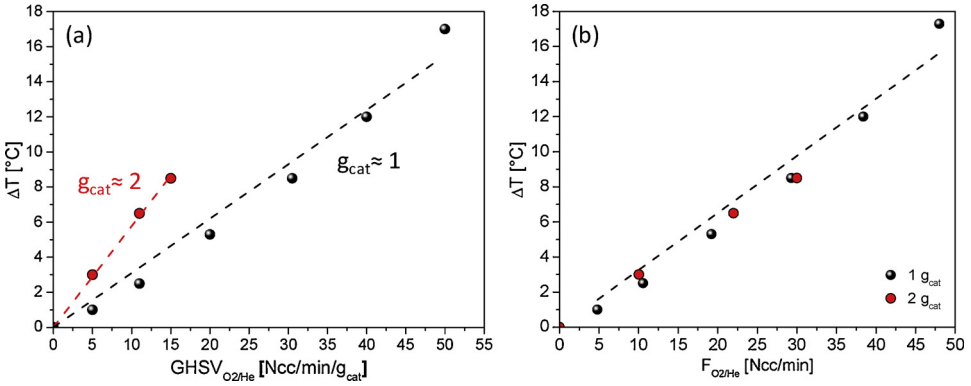

Fig. 8. Temperature gradient measured at the centerline of the catalyst bed obtained during the passivation treatment as a function (a) of the O_2 flow rate per unit mass of catalyst [Ncc/min/g_{cat}] and (b) of the O_2 flow rate [Ncc/min]. (For interpretation of the references to colour in this figure legend, the reader is referred to the web version of this article).

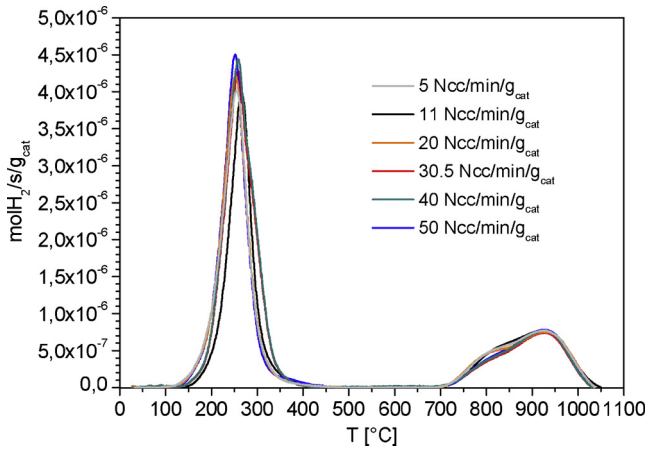

Fig. 10. H_2-TPR profiles of the samples passivated at different $GHSV_{O2/He}$ as a function of the temperature. (For interpretation of the references to colour in this figure legend, the reader is referred to the web version of this article).

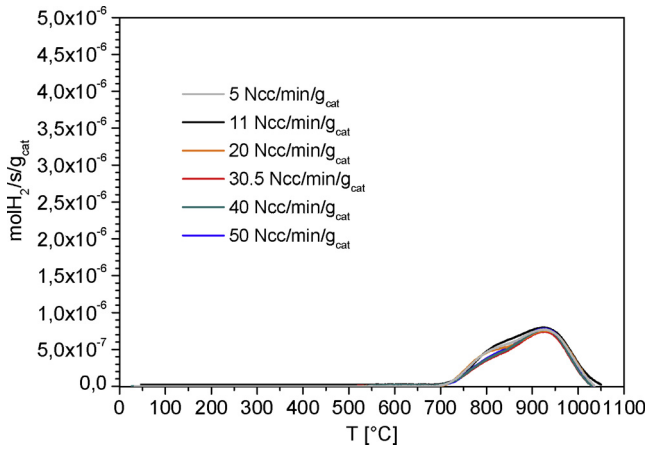

Fig. 11. H_2-TPR profiles of the samples passivated at different $GHSV_{O2/He}$ as a function of the temperature. (For interpretation of the references to colour in this figure legend, the reader is referred to the web version of this article).

exposure of the catalyst to air, thus suggesting the effectiveness of the catalyst passivation treatment.

As shown in Fig. 10, only one reducing peak with a maximum in the T-range of 250–260 °C is detected in the H_2-TPR profiles of all the passivated catalysts. The onset of the reduction peak is at around 120 °C and it is complete at 450 °C. No peaks are identified in the range 450–700 °C. The presence of only one peak suggests that mainly CoO species are formed during passivation, in line with recent works [9].

By assuming that the passivation layer is constituted by CoO, the degree of oxidation of the passivated samples (i.e. the $Co^{2+}/(Co^{\circ} + Co^{2+})$ ratio) can be calculated as the ratio between the amount of H_2 consumed to reduce the passivated catalysts (low-T peak in the TPR profiles of Fig. 10) and the theoretical amount of H_2 required to reduce the sample under the hypothesis that all the active Co is present as Co^{2+}. The degrees of oxidation of the catalysts passivated at 5, 11, 20, 30.5, 40 and 50 Ncc/min/g_{cat} are found to be 32.5, 32.3, 31.9, 31.0, 29.9 and 30.2%, respectively. This means that in the passivated samples around 70% of cobalt is still present in the metallic form. Theoretical estimations assuming the cobalt crystallites as spheres with diameter of 8.3 nm result in shell and core crystals having a metallic core of 5.8 nm in diameter and a CoO shell of 1.2 nm thickness, which is similar to that reported for similar passivation treatments [9]. This is also in line with the fact that CoO particles of such a small size are hardly detectable by XRD analysis.

The high-temperature peaks visible in the TPR spectra of Fig. 10 are attributed to the reduction of the Co-aluminates species used for the support stabilization are still present, thus indicating that these species are not affected by the passivation treatment, as expected.

As clearly shown in Fig. 10, the onset of the reduction of the CoO species formed during passivation occurs at significantly lower temperatures if compared with the calcined catalyst. This result is in line with that recently observed by Wolf et al. on passivated Pt-promoted Co/SiO_2 catalysts [9]. The authors attributed the improvement of the reducibility of the passivated catalysts to the presence of the metallic cobalt core having a beneficial effect on the reduction of the passivated catalysts. Hydrogen activation on this metallic surface could therefore take place at significantly lower reduction temperatures thus enhancing this process [9]. Furthermore, the thinner amorphous or more porous CoO layer formed upon passivation may be more easily reducible than the well crystallized CoO phase formed during the reduction of the calcined catalyst. Another explanation may be related to the inhibiting effect of Co_3O_4 in the reduction of CoO to Co°, that does not occur until the reduction from Co_3O_4 to CoO is completed [18,20]. In the passivated samples there is no evidence for the presence of Co_3O_4, and hence the CoO reduction may occur at significantly lower temperatures.

3.5. Characterization of the passivated catalysts after depassivation at 300 °C and at 400 °C

H_2-TPR analysis were also carried out on the samples after depassivation at 300 °C (Fig. 11) and 400 °C (not shown). At both these temperatures the depassivated samples show the presence of Co metal only, since no H_2 consumption was observed during the TPR. The complete reduction obtained by depassivating the passivated catalysts already at 300 °C is of particular interest because it indicates that the adoption of passivated catalysts allows the in-situ reduction of the catalyst at temperatures lower than those required for the calcined catalyst.

H_2-chemisorption analyses were carried out on all samples after depassivation at 400 °C. The Co° dispersion of the samples passivated with a $GHSV_{O2/He}$ of 5, 11 and 20 Ncc/min/g_{cat} is close to 12% and is similar to that obtained after reduction of the calcined catalyst at 400 °C (11.6%) (Table 2). This indicates that using appropriate passivation treatment does not have any effect on the morphology (i.e. Co° crystallites size distribution) of the catalyst.

At variance, when the samples are passivated at higher $GHSV_{O2/He}$ (30.5, 40 and 50 Ncc/min/g_{cat}) the Co metal surface slightly decreases and calculated Co° dispersion (D, Eq. (1)) is near 10, 8.4 and 7.8%, respectively (Table 2). Since these catalysts are fully reduced, the decrease of the Co° dispersion suggests the shift of the Co° crystallites size distribution to bigger values. As a matter of fact, the average Co° size calculated by Eq. (2) is 9.6, 11.4 and 12.3 nm, respectively (Table 2). This suggests the occurrence of Co° sintering at high space velocity of the passivation step, possibly due to the abrupt increase of the catalyst temperature observed during passivation (Fig. 7). The increase of the Co° size at higher O_2 space velocities may explain the slight decrease of the total moles of O_2 consumed by the catalyst (Fig. 6) during passivation.

H_2-chemisorption analysis after depassivation at 300 °C were also performed on the catalyst passivated at low O_2 flows ($GHSV_{O2/He}$ of 5, 11 and 20 Ncc/min/g_{cat}). Notably, a Co° dispersion (D, Eq. (1)) of 11.5% is still obtained in both the samples (Table 2), thus confirming the similarity between these samples and the calcined catalyst reduced at standard reduction conditions.

3.6. Stability to reoxidation with time of the passivated catalysts

One of the issues of the passivation process is the “stability” to reoxidation of the Co° core protected by the CoO passivation layer. In this regard, it is reported that the oxidation in air of a passivated catalyst is a spontaneous reaction dominated by a diffusion of oxygen to the cobalt

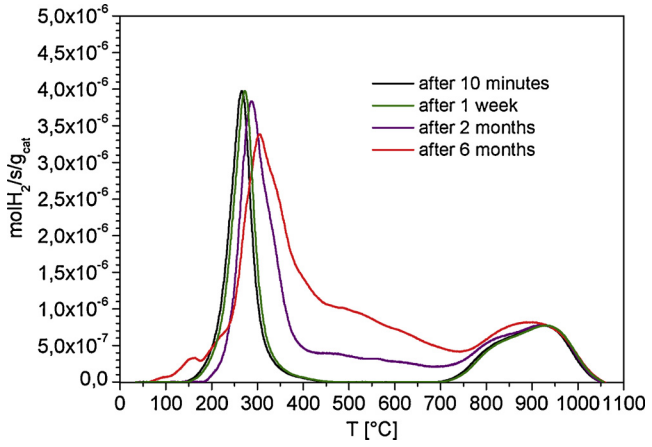

Fig. 12. H_2-TPR analysis on the samples passivated with a $GHSV_{O2/He}$ of 11 Ncc/min/g_{cat} (black line) after one week (green line), two months (violet line) and six months (red line) as a function of the time. (For interpretation of the references to colour in this figure legend, the reader is referred to the web version of this article.)

core and a radial growth of the oxide layer from the particle surface to the core [17].

The stability of our passivated catalysts was checked by repeating the H_2-TPR analysis upon passivation at $GHSV_{O2/He}$ of 11 Ncc/min/g_{cat} after one week, two months and six months of air exposure, and the results are shown in Fig. 12.

The TPR profile of the sample after one week is similar to that obtained immediately after passivation, thus indicating that a further oxidation of the Co° species did not occur during this period of time. At variance, in the TPR profile of the sample after two months the low-T reduction peak near 300 °C is broader and is shifted towards higher temperatures. Besides, a shoulder near 500 °C is also apparent. A more marked effect is seen by repeating the analysis after six months of air exposure. Based on the amounts of consumed H_2, Co_3O_4 must be formed in addition to CoO in these cases. Accordingly a complex picture is expected to be present in these cases, with the presence of CoO, Co_3O_4 and likely of Co° as well. This leads to a complex behaviour upon reduction of the catalyst. In particular the presence of Co_3O_4 may be responsible for the shift towards higher temperature of the first reduction peak and of the shoulder at 500 °C, in line with the inhibition of Co_3O_4 on the reduction of the CoO phase [18,20]. In any case, these results point out that the passivation treatment is not suitable for long-term protection as the catalyst experiences a progressive slow oxidation.

3.7. Catalyst testing

The performances of the calcined $Co/Pt/Al_2O_3^{(s)}$ catalyst reduced in-situ at standard reduction conditions were compared with those of the same catalyst reduced ex-situ at 400 °C, passivated with a $GHSV_{O2/He}$ of 11 Ncc/min/g_{cat}, exposed to air for two days and then depassivated in-situ at a lower temperature of 300 °C. The samples will be named $Co/Pt/Al_2O_3^{(s)}$(CR) and $Co/Pt/Al_2O_3^{(s)}$(RPD), respectively.

The catalytic performances were measured at 200 °C, 25 bar, H_2/CO inlet molar ratio = 2.0, SV = 83.33 Ncc/min/g_{cat}, inerts (N_2 + Ar) in the feed = 24 vol.% for around 100 h on stream.

Both catalysts were found to be very stable with Time on Stream (T.o.S.) in terms of activity and selectivity (Table 3). This is in contrast with previous studies showing a slight deactivation of the O_2-passivated catalysts [8]. The small decrease in activity of the O_2-passivated catalyst was attributed to the formation of irreducible cobalt species (like Co-aluminates) during the depassivation [8]. In this regard, we believe that the high stability of both our catalysts (reduced in-situ and passivated and depassivated) is related to the support stabilization, which reduces the interactions between Al_2O_3 and cobalt [19,20].

Notably, the two catalysts exhibited the same catalytic performances in the FTS (Table 2). In particular, the CH_4 selectivity is around 8%, the CO_2 selectivity is close to 0.3%, and the selectivity to C_{25+} and C_{5+} is 14 and 77%, respectively. This is well evident also in the Anderson-Schulz-Flory (ASF) plots shown in Fig. 13. Both distributions show the typical positive and negative deviations from the ideal linear distribution for methane and C_2 hydrocarbons, respectively, and a change of slope at a carbon number around 8. The chain growth probability for the C_{15+} species (α_{C15+}) is 0.877 for both catalysts. In line with the previous results, also the olefin to paraffin ratio trend is similar for both catalysts.

Noteworthy, the $Co/Pt/Al_2O_3^{(s)}$(RPD) catalyst was able to completely recover the catalytic performances of the $Co/Pt/Al_2O_3^{(s)}$(CR) catalyst, both in terms of activity and selectivity, even if depassivated at a significantly lower temperature.

The results obtained in terms of catalytic performances are a clear indication of the fact that milder in-situ activation conditions can be used in the presence of a reduced and passivated Pt-promoted Co-based Fischer-Tropsch catalyst.

4. Conclusions

The activation and passivation of a $Co/Pt/Al_2O_3^{(s)}$ Fischer-Tropsch catalyst were extensively studied in this work. Upon activation, the Co_3O_4 species of the calcined $Co/Pt/Al_2O_3^{(s)}$ catalyst were fully converted into Co° after reduction at standard reduction conditions (i.e. at 400 °C (heating ramp: 2 °C/min) for 17 h under a flow of pure H_2 (83.33 Ncc/min/g_{cat})). By decreasing the reduction temperature to 300 °C the reducibility of the catalyst decreased, as well as the number of Co metal surface sites available for the reaction.

The passivation of the $Co/Pt/Al_2O_3^{(s)}$ catalyst reduced at 400 °C was carried out at different space velocities of O_2/He (5, 11, 20, 30.5, 40 and 50 Ncc/min/g_{cat}) and by keeping constant the concentration of O_2 to 1 vol.%. All tests were repeated at least four times, showing great reproducibility. The O_2 profiles showed a typical adsorption trend, keeping at zero until a breakthrough time where a sudden transition to an asymptotic level equal to the inlet one occurs. The breakthrough time proportionally decreased on increasing the GHSV, consistently with a constant adsorption capacity. The specific amount of O_2 consumed ($molO_2^{cons}/g_{cat}$) after passivation slightly decreases with the increase of the space velocity.

The temperature measured at the center of the catalyst bed was monitored during the entire passivation step. We have found that the temperature gradients (ΔTs) measured on the catalyst bed linearly increased with the O_2 flow rate. This is in line with the occurrence of an exothermic phenomenon involving the complete consumption of O_2; these aspects should be carefully considered in view of the scalability of the passivation procedure.

All the passivated catalysts showed the presence of CoO species, whose reduction peak resulted shifted to lower temperatures if compared with the calcined sample. In line with this result, all the passivated samples could be fully reduced after depassivation at both 400 and 300 °C. However, different results were obtained in terms of number of Co° surface sites available for the FTS upon passivation at different space velocities. Indeed, while the Co° dispersion of the samples passivated with $GHSV_{O2/He}$ in the range 5–20 Ncc/min/g_{cat} was similar to that obtained with the calcined catalyst reduced at the same reduction temperature of 400 °C, that of the samples passivated at higher $GHSV_{O2/He}$ was lower. This was attributed to sintering phenomena of the CoO species occurring during passivation step at high spece velocity as a result of the abrupt increase of the catalyst temperature.

The passivated catalysts did not change after air exposure for one week, while they were significantly re-oxidized after few months, thus

Table 3
Catalysts stability with Time on Stream (T.o.S.). T = 200 °C, P = 25 bar, H_2/CO = 2.0 mol/mol, SV = 83.33 Ncc/min/g_{cat}, inerts in the feed (N_2 + Ar) = 24 vol.%.

$Co/Pt/Al_2O_3^{(s)}$(CR)						$Co/Pt/Al_2O_3^{(s)}$(RPD)					
T.o.S. [h]	COconv [%]	S_{CH4} [%]	S_{CO2} [%]	S_{C5+} [%]	S_{C25+} [%]	T.o.S. [h]	COconv [%]	S_{CH4} [%]	S_{CO2} [%]	S_{C5+} [%]	S_{C25+} [%]
24	19.9	8.3	0.2	–	–	24	19.6	8.0	0.2	–	–
50	20.1	8.1	0.3	77.0	14.0	50	19.4	8.3	0.3	77.0	14.0
74	19.9	8.2	0.3	77.0	14.0	74	19.1	8.5	0.3	76.9	13.9
102	19.9	8.1	0.3	77.1	14.0	102	19.1	8.5	0.3	77.0	14.0

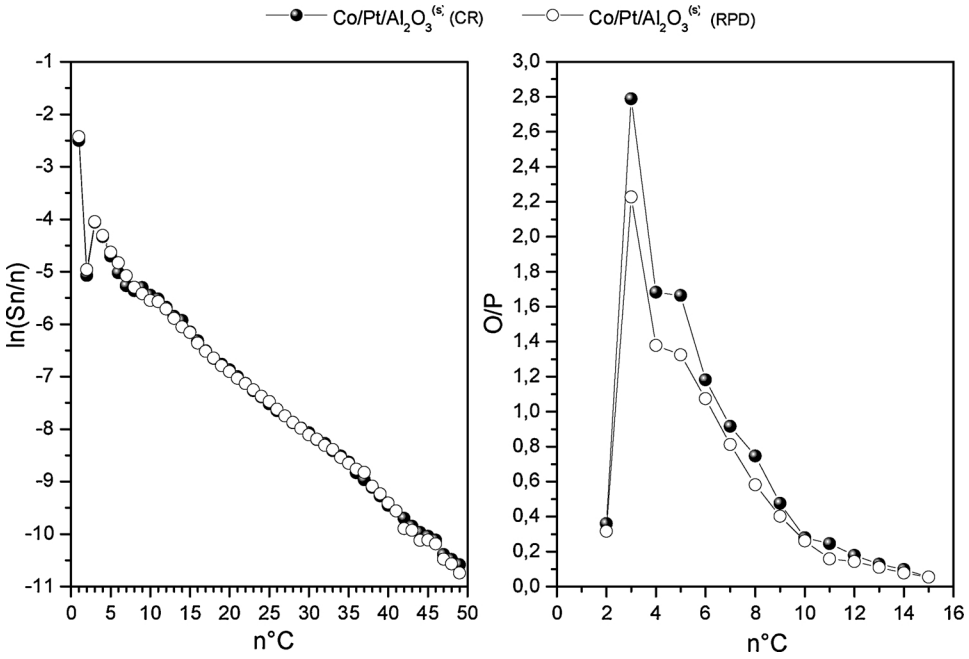

Fig. 13. ASF distributions (on the left) and olefin to paraffin ratio (on the right) of the catalysts as a function of the carbon number (n). p.c.: T = 200 °C, P = 25 bar, H_2/CO = 2.0 mol/mol, SV = 83.33 Ncc/min/g_{cat}, inerts in the feed (N_2 + Ar) = 24 vol.%, T.o.S = 74 h.

indicating that the passivation treatment was not suitable for long-term catalyst protection.

The effectiveness of the catalyst passivation was eventually validated by running FT reactivity tests at industrially relevant process conditions. The $Co/Pt/Al_2O_3^{(s)}$ catalyst was reduced at standard reduction conditions ex-situ and then passivated with a $GHSV_{O2/He}$ of 11 Ncc/min/g_{cat}. Then, it was transferred into the FTS unit and depassivated in-situ at 300 °C. Its activity was compared with that obtained by in-situ reducing the calcined catalyst at standard reduction conditions (400 °C). Interestingly, the same catalytic performances, expressed both in terms of activity and selectivity, were obtained. Furthermore, both the catalysts were stable for several hours of T.o.S.

The results obtained in this work are a clear evidence that the passivation treatment may provide an effective solution to all the issues linked to performing the catalyst activation in the same reactor used for running the reaction.

Acknowledgments

The research leading to these results has received funding from the European Research Council under the European Union's Horizon 2020 research and innovation program (Grant Agreement no. 694910/ INTENT).

References

[1] C.J. Weststrate, M.M. Hauman, D.J. Moodley, A.M. Saib, E. van Steen, J.W. Niemantsverdriet, Top. Catal. 54 (2011) 811–816.
[2] G. Jacobs, Y. Ji, B.H. Davis, D. Cronauer, A.J. Kropf, C.L. Marshall, Appl. Catal. A-Gen. 333 (2007) 177–191.
[3] H. Van Rensburg, WO2014064563A1.
[4] P. Chaumette, A. Gusso, R. Zennaro, EP0934115B1.
[5] C.L. Kibby, A. Haas, US20100168258A1.
[6] G. R. Wilson, N. L. Carr, US005639798A.
[7] S. Eri, E. Rytter, R. Mystrad, EP259578A2.
[8] S. Hammache, J.G. Goodwin Jr, R. Oukaci, Catal. Today 71 (2002) 361–367.
[9] M. Wolf, N. Fischer, M. Claeys, Catal. Today 275 (2016) 135–140.
[10] E. Iglesia, S.L. Soled, R.A. Fiato, J. Catal. 137 (1992) 212–224.
[11] M.W.J. Crajé, A.M. van der Kraan, J. van de Loosdrecht, P.J. van Berge, Catal. Today 71 (2002) 369–379.
[12] G.L. Bezemer, J.H. Bitter, H.P.C.E. Kuipers, H. Oosterbeek, J.E. Holewijn, X. Xu, F. Kapteijn, A.J. van Dillen, K.P. de Jong, J. Am. Chem. Soc. 128 (2006) 3956–3964.
[13] M.K. Gnanamani, G. Jacobs, W.D. Shafer, B.H. Davis, Catal. Today 215 (2013) 13–17.
[14] N. Fischer, B. Clapham, T. Feltes, M. Claeys, ACS Catal. 5 (2015) 113–121.
[15] D. Srikala, V.N. Singh, A. Banerjee, B.R. Mehta, S. Patnaik, J. Phys. Chem. C 112 (2008) 13882–13885.
[16] M.A. Zalich, V.V. Baranauskas, J.S. Riffle, M. Saunders, T.G.St. Pierre, Chem. Mater. 18 (2006) 2648–2655.
[17] C. Dobbrow, A.M. Schmidt, Beilstein J. Nanotechnol. 3 (2012) 75–81.
[18] L. Fratalocchi, C.G. Visconti, L. Lietti, N. Fischer, M. Claeys, submitted to Catal. Sci. Technol. (2019).
[19] L. Fratalocchi, C.G. Visconti, L. Lietti, G. Groppi, E. Tronconi, E. Roccaro, R. Zennaro, Catal. Sci. Technol. 6 (2016) 6431–6440.
[20] L. Fratalocchi, C.G. Visconti, L. Lietti, N. Fischer, M. Claeys, Appl. Catal. A-Gen. 556 (2018) 92–103.
[21] D. Schanke, S. Vada, E.A. Blekkan, A.M. Hilmen, A. Hoff, A. Holmen, J. Catal. 156 (1995) 85–95.
[22] G. Jacobs, Y. Ji, B.H. Davis, D. Cronauer, A.J. Kropf, C.L. Marshall, Appl. Catal. A-Gen. 333 (2007) 177–191.
[23] C.G. Visconti, M. Mascellaro, Catal. Today 214 (2013) 61–73.
[24] C.G. Visconti, L. Lietti, P. Forzatti, R. Zennaro, Appl. Catal. A-Gen. 330 (2007) 49–56.
[25] D. Schanke, S. Vada, E.A. Blekkan, A.M. Hilmen, A. Hoff, A. Holmen, J. Catal. 156 (1995) 85–95.
[26] D. Nabaho, J.W.H. Niemantsverdriet, M. Claeys, E. van Steen, Catal. Today 261 (2016) 17–27.